Broadband cavity-enhanced optical flux monitoring

Roman Rousseau, Claude Botella, Jérôme Morville, Mohamed Bounab, Lotfi Berguiga, Clarisse Furgeaud, Romain Bachelet, Guillaume Saint-Girons

Broadband cavity-enhanced optical flux monitoring

Roman Rousseau[1], Claude Botella[1], Jérôme Morville[2], Mohamed Bounab[1], Lotfi Berguiga[1], Clarisse Furgeaud[1], Romain Bachelet[1] and Guillaume Saint-Girons[1*]

[1]*INL-UMR5270/CNRS, Ecole Centrale de Lyon, 36 avenue Guy de Collongue 69134 Ecully cedex, France*

[2]*ILM-UMR5306/CNRS, UCBL, 10 rue Ada Byron 69622 Villeurbanne cedex, France*

*guillaume.saint-girons@ec-lyon.fr

Abstract

This work describes a new type of sensor for growth process monitoring named broadband cavity-enhanced optical flux monitoring sensor (BBCE-OFM). Like existing optical flux monitoring solutions (OFM), it relies on absorption spectroscopy. However, the implementation of an optical cavity reduces the measurement uncertainty, enabling efficient operation even at very low growth rates. Using the BBCE-OFM sensor mounted in our solid-source oxide MBE reactor, we achieved an uncertainty of ±2% on the measurement of Sr and Ti growth rates in $SrTiO_3$ at around 1 ML/min, to be compared to the ±16% obtained in the same conditions using a conventional OFM setup. Furthermore, our sensor architecture, based on an echelle monochromator and LEDs replacing the hollow cathode lamps (HCLs) used in standard OFM sensors, is more robust against drift.

Introduction

Thin film deposition processes are at the heart of a variety of technologies (coatings for optics, chemistry, surface treatments, micro/optoelectronics,…).[1] In most of these fields, and for micro/optoelectronics in particular, the development of thin film deposition control fuels progresses, and the specifications in terms of growth control are highly constrained. Complex epitaxial heterostructures (of semiconductors, oxides, …) controlled down to the monolayer (ML) scale must be reproducibly fabricated by minimizing operating losses (non-compliant wafers/batches) and production costs. This requires constant improvement of the accuracy, reliability and reproducibility of the deposition processes.

In such processes, controlling the growth rate is essential to control the composition and thickness of the films. In most practical cases, this control is carried out by measuring ex-situ the composition and thickness of dedicated calibration samples, further growths being performed under the hypothesis of stable sources. Source stability is however limited by many factors. In molecular beam epitaxy (MBE) reactors for instance, the metal loads evaporated in the effusion cells evolve during the process (change in size and shape, reactions with the growth ambient[2]) causing drift and instabilities that necessitate frequent recalibrations. This represents significant cost and time expense, and limits the accuracy with which the process is controlled. *In-situ* measurements carried out before the growth (measurement of the molecular beam equivalent pressure using Bayard-Alpert gauges, growth rate measurement using quartz microbalances (QCM), …) help correcting source drift from one day to the next, but are inefficient at correcting drift occurring during the growth. Correcting such drift requires the use of a sensor able to measure the growth rate in real time, coupled to feedback loops on the sources, to actively compensate growth rate variations during the process. Such a real-time sensor must be accurate enough to meet the constrained specifications of the deposition processes, and be reliable and reproducible. It must also present a limited footprint to avoid substrate shadowing, and be operable in the various ambients used in growth processes (oxygen for oxides, nitrogen for nitrides, As or P vapors for III-V, vector gas, …). In the end it must enable the simultaneous measurement of the growth rate of several elements, for compound composition control.

Developing such a sensor has been the subject of significant efforts, but none of the available tools satisfies the specifications mentioned above. Mass spectroscopy[3] uses bulky measurement heads likely to cause substrate shadowing and is disturbed by ambient gases (V elements background pressure in III-V growth processes, O_2 background pressure in oxide growth processes,…)[4]. So is electron impact emission spectroscopy (EIES), which also presents a limited sensitivity[5]. In the end, quartz crystal microbalances (QCM) are not chemically selective and are therefore intrinsically single channel. Their

response is highly sensitive to temperature variations. In comparison to these techniques, so called optical flux monitoring sensors (OFM) present several advantages. Their basic principle relies on the measurement of the absorbance of the gas phase surrounding the substrate, which relates to the growth rate[6]. The absorbance is derived from the Beer-Lambert law, which requires measuring the absorbed intensity I_{abs} and the unabsorbed (reference) intensity I_{ref}. Standard OFM sensors use hollow cathode lamps (HCLs) as light sources, because the spectrum of the latter is spectrally very close to the absorption lines to be measured[7–10]. This overcomes the issue of the narrow spectral width of these lines, which is difficult to resolve with standard monochromators. Contrasting with most of their competing techniques, OFM sensors are not disturbed by ambient gases and do not cause any substrate shadowing (both the source and the detection systems are mounted outside the reactor). However, as the HCL spectrum consists in an ensemble of discrete lines over a zero baseline, the latter cannot be used to measure the reference intensity I_{ref}, contrasting with what is done in many atomic absorption spectroscopy systems[11]. Instead, an optical path different from that used to measure I_{abs} is used to assess I_{ref}, so that both channels undergo different fluctuations (dilatation and parasitic coverage of the viewports of the signal channel, for instance). This causes a drift of typically 1 to 3% per hour [12], thus affecting the accuracy and the reproducibility of the sensor[12–14]. Several strategies have been proposed to extract I_{ref} and I_{abs} from beams passing through a single optical channel. In so-called "pseudo-double beam" OFM sensors, the incident atom flux is chopped using the reactor shutters, and I_{abs} (respectively I_{ref}) is measured when the shutter is open (respectively closed)[15]. This solution is efficient for drift correction but imposes a shuttered growth sequence which is barely compatible with many growth processes. In "self-corrected" OFM sensors, I_{ref} is measured using an unabsorbed line emitted by the HCL (line emitted by the noble gas)[16]. Efficiency for drift correction is limited (a drift of 1.7%/hour is reported in Ref.[16]), possibly due to the fact that both transitions are spectrally separated and are hence not efficient at compensating wavelength dependent optical path fluctuations. In the end; in "COPACT" (common optical path for automatic correction of transmission) OFM sensors, the light emitted by a broadband source (typically a LED or an arc lamp) is injected in the signal channel in addition to the light emitted by the HCL[4,17]. It is absorbed by the vapor but as the spectral width of the absorption line is much smaller than that of the broadband source, the resulting attenuation is negligible, so that it can be used to measure I_{ref}. This strategy enables good long term stability but imposes quite complex sensor architecture. In fact, two channels are required for each element to be measured and for the broadband source: the first one, passing through the reactor, is used to measure I_{abs}, and the second one, passing outside the reactor, is used to compensate source intensity fluctuations. Another major drawback of OFM sensors is their relatively high uncertainty, particularly at moderated and low growth rate. Although reasonable at high growth rates of ~1 ML/s

(in the 0.5 – 1 % range for ~1 s exposure time[17]), the relative uncertainty increases rapidly with decreasing growth rate to reach values as high as ~5% at 0.1 ML/s, [17] and >30% around 0.01 ML/s (for ~1 s exposure time) (section 3), incompatible with the specifications of most deposition processes.

In this work, we introduce a new concept of broadband cavity-enhanced optical flux monitoring sensor (BBCE-OFM) whose uncertainty outperforms that of conventional OFM sensors, and whose operating principle is more robust against drift. The sensor described here is designed to measure the growth rate of Sr and Ti for $SrTiO_3$ (STO) growth control in an oxide MBE reactor. This application is particularly relevant to evaluate the performance of our sensor, as the growth rate is low (the typical STO MBE growth rate is in the order of a few ML/min) and strongly subjected to drift due to the oxidation of the Sr and Ti loads inside the effusion cells during the process[2]. The sensor architecture is described in section 1. It includes an echelle monochromator whose spectral resolution is close to the broadening of the absorption lines to be measured. This allows to replace the HCLs used in standard OFM sensors by broadband sources such as LEDs. This configuration gives access to the spectral shape of the signal which confers on our sensor a number of advantages over conventional OFM sensors, as detailed in section 2. Additionally, an optical cavity, similar to that used in high sensitivity gas sensors,[18] allows to considerably increase the interaction length between the atomic beams and the light, which boosts the sensor sensitivity as demonstrated in section 3.

1. The BBCE-OFM setup

A schematic of the BBCE-OFM sensor mounted in our oxide (MBE) reactor is displayed in Fig.1. Ti (respectively Sr) growth rate is monitored using the absorption line centered around 399.98 nm (respectively 460.86 nm).

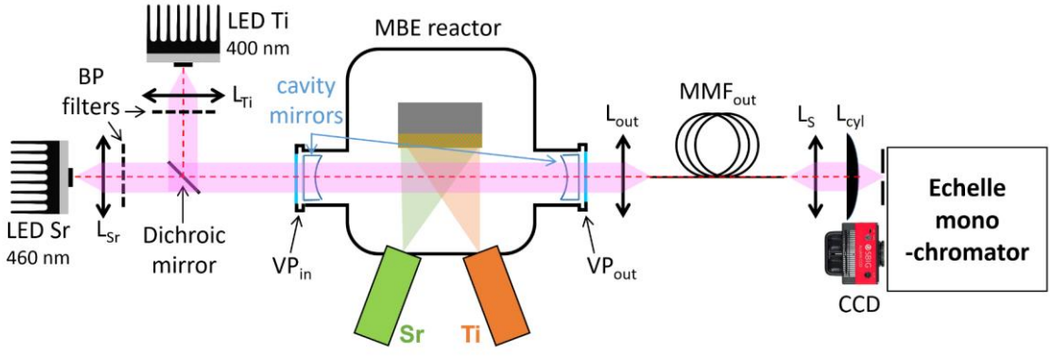

***Fig.1** : schematic of the BBCE-OFM sensor.*

The light emitted by the two LEDs (central wavelengths 400 and 460 nm) is collimated using aspheric lenses (L_{Ti} and L_{Sr}), filtered spectrally using 10 nm bandwidth bandpass filters (BP filters) centered around the LED central wavelengths, and aligned along a single optical axis using a dichroic mirror (425nm cut-on wavelength). This beam enters the reactor through the input viewport VP_{in} (antireflection-coated fused silica viewport). The light is then coupled into a 1.7m-long optical resonant cavity formed by two high-reflectivity dielectric mirrors (reflectivity R = 99.8 ±0.05% in the 350-560 nm range) placed inside the reactor, right after the viewports, on either side of the molecular beams emitted by the effusion cells. The light transmitted by the optical cavity passes through the output viewport VP_{out} (identical to VP_{in}) and is coupled in the output fiber MMF_{out} (multimode fiber, 10m-long, 200 µm core diameter, 0.22 NA (numerical aperture)). At the MMF_{out} output, the light is focused on the entrance slit of an Ebert-Fastie echelle monochromator (SOPRA UHRS F1500, 1500mm focal length) using an aspheric lens L_s (focal length f=30 mm) and a cylindrical lens L_{cyl} (f=75 mm). The light is collected at the monochromator exit using a CCD camera (SBIG Aluma 8300), cooled at -20°C to reduce the dark current contribution. The monochromator is equipped with a curved entrance slit to limit astigmatism[19] and a R2 echelle grating (blaze angle $\theta_B = 63.43°$, groove density $G = 98.76\ mm^{-1}$).

Both high-reflectivity mirrors are mounted on fine tilt stages (angular resolution <1 mrad) enabling resonant cavity alignment. To probe this alignment, measure the mirror reflectivity and assess the mechanical stability of the cavity, a specific cavity ringdown spectroscopy (CRDS) setup was developed (not detailed here). Such a setup allows to measure the photon lifetime in the cavity, which is very sensitive to the cavity alignment and the mirror reflectivity.[20] A photon lifetime of 2.35 µs was measured at 400 nm, corresponding to a mirror reflectivity R=99.75%, very close to the nominal value. Long term continuous CRDS monitoring during MBE operations revealed excellent stability of the photon lifetime, demonstrating a very good stability of the cavity. This shows in particular that the latter is not affected by the MBE environment. The stability is enhanced by the fact that the mirrors are mechanically linked to the reactor, and are therefore subject to the same vibrations as the latter, caused in particular by the turbomolecular pump. Above all, the LEDs used as light sources present broadband spectra and much larger etendues than that of the cavity. This reduces the sensitivity of the LED/cavity optical coupling to misalignment, and hence to mechanical instabilities. Besides, the stability of the photon lifetime also shows that the mirrors remain clean and free of any parasitic material deposition in our growth conditions.

2. Spectral properties of the signal, extraction of I_{abs} and I_{ref}

As mentioned in the introduction, the narrow spectral width of the absorption lines to be measured (about 0.1 to 1 pm[21,22]) is a challenge for OFM sensor design. In standard OFM sensors, this challenge is addressed using HCL light sources, whose spectral width (typically 1.5 pm[8–10]) comes close to the absorption line broadening. Such sensors measure the attenuation of the HCL emission line chosen for the analysis caused by the gas phase absorption without measuring the signal spectrum. In our BBCE-OFM sensor, a high spectral resolution is provided by the echelle monochromator. Using HCLs is therefore no longer essential. They can be replaced by broadband sources such as the LEDs used in this work. This configuration (broadband source combined with a high-resolution echelle monochromator) enables a continuous spectrum to be measured around the absorption line, which, as detailed in this section, provides significant advantages and implies a few precautions regarding the sensor design.

Contrasting with standard blazed gratings usually optimized for the first or second diffraction order, echelle gratings operate at high diffraction order m (typically 20 to 80) due to their high blaze angle. This enables very high spectral resolution, as the resolving power of the grating scales with the diffraction order for a given wavelength[23]. According to our measurements (SM section SM2), the echelle monochromator used for our sensor has an ultimate resolution of 1 pm (obtained with a 10 µm entrance slit width), approaching the absorption line spectral width. Yet the effect of slit width on the sensor SNR results from a tradeoff between spectral resolution (enhanced by low slit widths) and photon flux on the CCD (which increases as slit width increases. Our measures showed that using a 100 µm entrance slit width is the best compromise to maximize the sensor SNR. With such an entrance slit width, the monochromator resolution is 8 pm (SM section SM2). Besides, the free spectral range (FSR) of a monochromator (spectral range for which superimposition of light from adjacent diffraction orders of a grating does not occur) is inversely proportional to the diffraction order m (SM section SM2). It is thus very small for an echelle grating (in our experiment $FSR = 8.7\ nm$ for $\lambda = 400\ nm$ and $m = 46$), leading to a strong overlap of the light from adjacent diffraction orders on the monochromator output. This overlap is generally not desired, so that echelle gratings are commonly used in tandem with a dispersive element (prism or grating) called "cross-disperser", mounted perpendicular to the echelle grating. The cross disperser separates the different diffraction orders vertically in the monochromator output plane. This separation, achieved at the cost of a reduction of the monochromator etendue and therefore of the number of photons collected per wavelength on the detector, is unnecessary for our sensor. Indeed, the very narrow spectral width of the absorption lines make their spatial superimposition after the echelle grating very unlikely. We therefore do not use a secondary dispersive element in our sensor. Besides, the superimposition of the diffraction

orders makes it possible to simultaneously probe a wide spectral range without rotating the grating, facilitating simultaneous monitoring of several elements.

The image obtained on the CCD for $SrTiO_3$ growth rates of 3 ML/min and 1.5 ML/min, respectively, is shown in Fig.2(a).

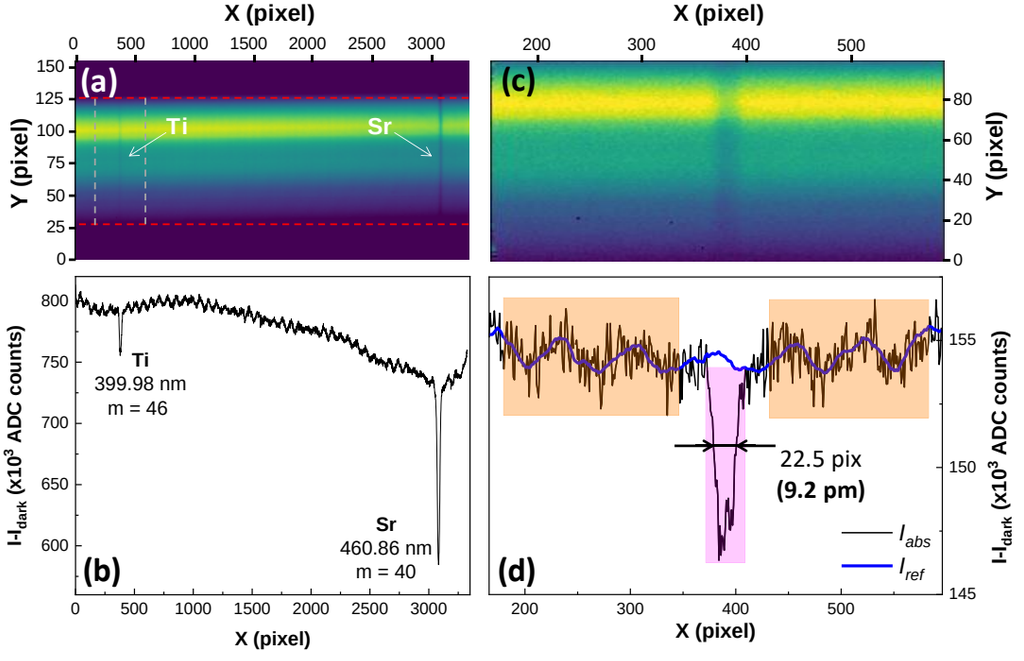

Fig.2 *: (a) Image recorded on the CCD for Sr and Ti growth rates in $SrTiO_3$ of about 3 ML/min and 1.5 ML/min, respectively (Sr cell temperature : 430°C, Ti cell temperature : 1800°C). The intensity corresponds to $I - I_{dark}$ where I is the measured intensity and I_{dark} is the intensity measured in the dark (CCD shutter closed) (b) Profile obtained by binning the image shown in (a) between the horizontal the dotted red lines. m indicates the diffraction order. (c) ROI centered around the Ti line (after slit curvature correction), defined by the vertical dotted grey lines in (a). (d) Profiles obtained by binning vertically the image. I_{abs} is obtained from (c). The orange regions from both sides of the absorption dip are that considered for the fit used to determine I_{ref}, and the absorption dip is integrated over the pink region.*

Diffraction order superimposition allows to simultaneously detect the Ti line at 400 nm (diffraction order 46) and the Sr line at 460 nm (diffraction order 40) on the CCD without rotating the grating. A region of interest (ROI) extracted from Fig.2(a) centered around the Ti line is shown in Fig.2(c). In this image, the curvature of the monochromator entrance slit has been corrected numerically to avoid the degradation of spectral resolution when vertically binning the image. The profile after vertical binning is shown in Fig.2(d). The full width at half maximum of the Ti absorption dip is 22.5 pixels, which corresponds to 9.2 pm. This value is close to the spectral resolution of the monochromator (8 pm with

100 µm entrance slit width) showing that the spectral width is largely dominated by the instrumental broadening.

In standard OFM sensors, the wavenumber (σ) dependant absorbance $A(\sigma)$ relates to I_{ref} and I_{abs} as $A(\sigma) = 1 - \frac{I_{abs}}{I_{ref}}(\sigma)$. By analogy, we define for our BBCE-OFM sensor the effective absorbance $A_{eff}(\sigma)$ as

$$A_{eff}(\sigma) = 1 - \frac{I_{abs}}{I_{ref}}(\sigma). \quad (Eq.1)$$

$A_{eff}(\sigma)$ depends on the cavity mirror reflectivity R and on the monochromator resolution. The absorbed intensity $I_{abs}(\sigma)$ and the unabsorbed (reference) intensity $I_{ref}(\sigma)$ can be both extracted from the profile displayed in Fig.2(d). $I_{ref}(\sigma)$ corresponds to the profile baseline. It is obtained by fitting the signal outside the absorption dip using a suitable function, noted f_{BL}. This function is then used to extrapolate I_{ref} in the spectral range of the absorption dip. The baseline shows interferences whose period corresponds to a millimeter-thick Fabry-Perot cavity (for an optical index of 1.5), probably formed by the spectral filters placed in front of the LEDs. To closely describe these interferences, a preliminary measurement is made by closing the effusion cell shutters to remove the contribution of the absorption dip. The resulting signal is smoothed to remove noise. Then, during the sensor operation with open effusion cell shutters, f_{BL} is obtained by adding a 3rd order polynomial to this smoothed signal, after application of a spectral shift to it. The polynomial describes slow baseline variations, while the spectral shift describes any shift of the interferences caused, for instance, by slight temperature changes of the filters in front of the LEDs. For each measurement, the spectral shift and the polynomial coefficients are fitted to adjust f_{BL} to the experimental data outside the absorption dip (orange regions in Fig.2(d)), and f_{BL} is then used with these fitted parameters to determine I_{ref} over the entire ROI spectral range (blue curve in Fig.2(d)).

Diffraction order superimposition at monochromator exit must be considered to maximize the effective absorbance, as illustrated in Fig.3 and explained below.

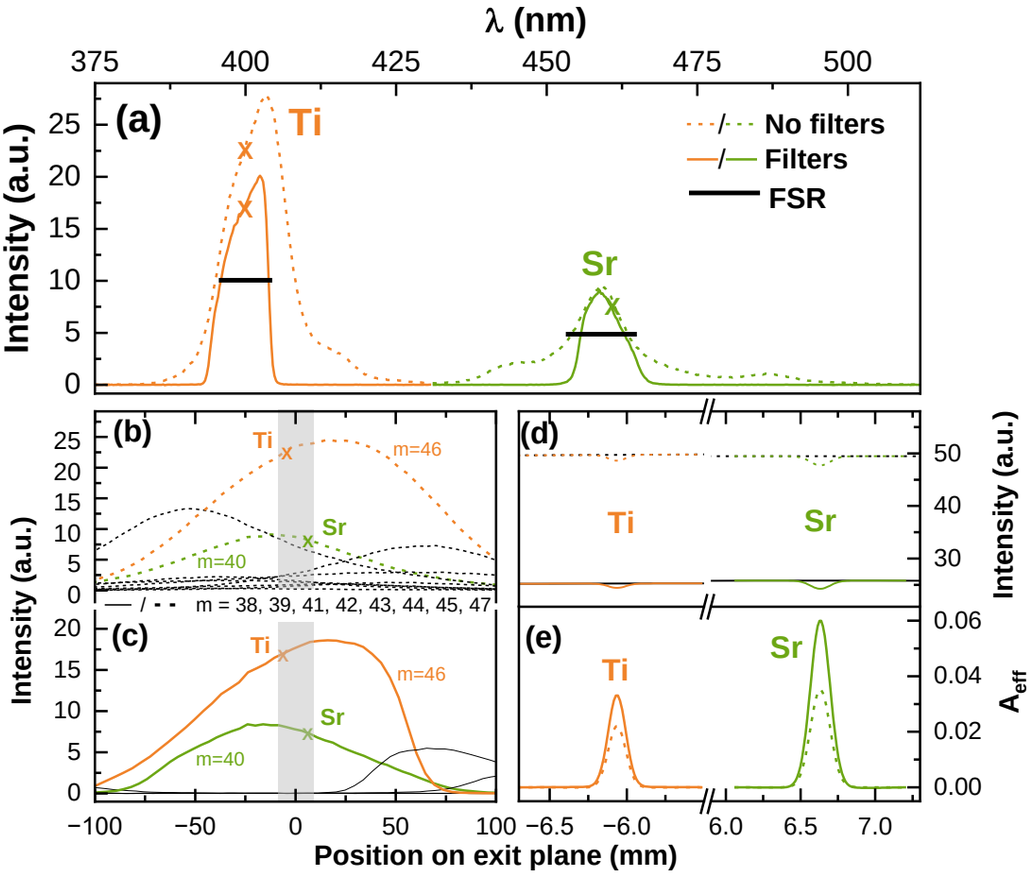

Fig.3 *(a) Spectrum at MMF_{out} output with and without the BP filters recorded with a Teledyne Isoplane 81 spectrometer (resolution ~1nm). The free spectral range (FSR) of the echelle monochromator near the maximum emission wavelength of each LED is indicated by black bars, and the crosses indicate the positions of the Ti and Sr absorption lines. (b) and (c) Simulated spatial distribution of the light intensity on the exit plane of the monochromator for the different diffraction orders without (b) and with (c) the BP filters using the spectra from (a). Crosses indicate the positions of the Ti and Sr absorption lines, respectively diffracted at order 46 and 40. The black curves correspond to adjacent diffraction orders without Sr and Ti absorption lines. The gray transparent rectangle indicates the extension of the CCD. (d) Calculated CCD signal without (dashed lines) and without (continuous lines) BP filters (sum of the contributions of the different diffraction orders displayed in (b) and (c)). Sr and Ti absorption dips are calculated for a STO growth rate of 1 ML/min by considering the monochromator instrumental function, as described in SM section SM4. (e) A_{eff} calculated for Sr and Ti without (dashed lines) and with (continuous lines) BP filters.*

To measure the spectrum of the light injected in the echelle monochromator, we used a medium-resolution spectrometer operating at order 1 (Princeton Instrument Teledyne Isoplane 81). The measurement was performed with the BP filters (in the configuration used for sensor), and without the BP filters, for comparison (Fig.3(a)). From these spectra, we calculated in both cases the spatial distribution of the light intensity at the output of the echelle monochromator depending on the

diffraction order (Fig.3(b) and (c), see SM section SM2 for calculation detail). The Ti and Sr absorption dips respectively appear on orders 46 and 40. In the end, the signal measured on the CCD, which corresponds to the sum of the contributions from all the diffraction orders, was also calculated (Fig.3(d)). Without filters, the light intensity is distributed over 8 diffraction orders (m=38 to 47). Adjacent diffraction orders corresponding to spectral ranges without the absorption lines of interest (black curves in Fig.3 (b)) represent a significant fraction of the output signal. In contrast, in our actual setup where BP filters are placed in front of each LED, the light intensity is only distributed over the two diffraction orders carrying the Sr and Ti absorption dips, namely m=46 and m=40, respectively. The contribution of the adjacent diffraction orders is negligible in the range covered by the CCD (Fig.3(c), gray area). As a result, the baseline intensity is reduced by a factor ~2 when BP filters are used (Fig3(d)), which enhances the effective absorption contrast A_{eff} (Fig3(e)).

In summary, the configuration of our BBCE-OFM sensor gives access to the spectral shape of the signal (convolved to the monochromator instrumental broadening), which confers on it a number of advantages over conventional OFM sensors. First, it allows to extract I_{ref} and I_{abs} using a single optical channel, eliminating an important cause for drift in standard OFM sensors. From this point of view, our sensor is comparable to COPACT OFM sensors. However, whereas COPACT sensors require an additional channel per source to correct for differential source intensity fluctuations, in our sensor the same reference signal I_{ref} corrects the for both optical path drift and source intensity fluctuations, which simplifies its architecture. Additionally, standard OFM sensors do not provide access to the signal spectrum, but only to spectrally integrated values. As a consequence, their response depends on the spectral overlap between the HCL lines and the absorption lines[13,24]. This overlap depends on the HCL emission linewidth, which in turn varies in particular with the HCL current and the HCL cathode fatigue[12,13]. It also depends on the absorption linewidth, which in turn varies with the effusion cell temperature and with the effusion cell filling rate dependent molecular beam divergence due to Doppler effect[25]. It is therefore likely to vary depending on the experimental conditions, causing significant drift[24]. In contrast, thanks the broadband light source and the echelle monochromator, our BBCE-OFM sensor provides access to a continuous spectrum. Thus, it does detect the shift and broadening of the absorption lines (SM section SM5), even if the latter are not resolved by the echelle monochromator. This is expected to limit the impact of these effects on sensor stability. Measuring the continuous spectrum also provides rich information on the baseline shape that can processed to tackle parasitic Fabry Perot interferences, as shown above for the extraction of I_{ref}. Such spectral information cannot be obtained in standard OFM sensors.

From a practical point of view, the main disadvantage of our setup is the size of the echelle monochromator. However, as explained in section 2, the optimal SNR is not obtained with the ultimate resolution of the monochromator (1 pm, with a 10 µm entrance slit aperture), but by opening the entrance slit to 100 µm, which corresponds to a resolution of 8 pm. The same resolution can be achieved with a monochromator equipped with the same grating, having a focal length divided by 2, by using a 50 µm entrance slit aperture. This means that the spectrometer footprint can be significantly reduced, while maintaining the required resolution. Also, our modified echelle spectrometer does not require a cross-disperser, which simplifies its design and alignment compared to conventional echelle monochromators. In the end, the LEDs used in our sensor are less expensive than HCLs, and have a longer lifetime. They are also more compact and easier to integrate into an optical system; and their intensity is more stable than that of the light emitted by HCLs. Their spectral radiance is significantly larger than that of HCLs, which enhances SNR as discussed in the next section.

3.Signal and signal to noise ratio as a function of the growth rate

While the broadband source and the echelle monochromator confer significant benefits on our sensor in terms of stability, the optical cavity enhances its SNR. Indeed, the light resonates in the optical cavity and travels through the molecular beams about 500 times compared to 1 or 2 passes in standard OFM sensors. The number of light roundtrips (given by $\frac{1}{2(1-R)}$, where R is the mirror reflectivity) increases with increasing mirror reflectivity, which in turn increases the effective absorbance. However, the transmission of the cavity decreases with increasing mirror reflectivity, which reduces the photon flux on the detector and also affects the noise regime. There is thus a trade-off in mirror reflectivity to maximize the SNR[26]. Furthermore, the geometric etendue of the echelle monochromator is relatively small, which also leads to a reduction of the spectral photon flux on the detector compared with standard OFM sensors. This reduction is compensated by the spectral radiance of the LEDs, which is higher than that typical of HCLs (SM section SM3). The above comparison between standard OFM and our BBCE-OFM sensor remains qualitative. Indeed, a more quantitative comparison would require to have both sensors thoroughly optimized in terms of light sources, optical path spectrometer design, etc…. It is therefore quite complex and will be conducted in a future article. In the following, we show that, overall, our BBCE-OFM sensor offers a significant improvement in measurement uncertainty compared with standard OFM sensors.

The sensor signal, defined as

$$S_{BBCE} = \int_{-\infty}^{\infty} A_{eff}(\sigma) d\sigma, \quad (Eq. 2)$$

was measured as a function of the Sr and Ti growth rates in STO (GR) by varying the Sr and Ti effusion cell temperatures (more details in SM, section SM6). For this purpose, CCD images similar to that shown in Fig.2 were recorded using an exposure time of 1s, and treated in real time using a LabVIEW interface to extract I_{ref} and I_{abs} using the procedure described in the previous section. S_{BBCE} was then derived by integrating the experimental signal in the pink region of Fig.2(d)

$$S_{BBCE} = \Delta_{pix} \sum_{pixel\ in\ pink\ region} \left[1 - \frac{I_{abs}}{I_{ref}}\ (pixel)\right], \qquad (Eq.3)$$

with Δ_{pix} the pixel spectral width ($\Delta_{pix} = 0.023\ cm^{-1}$). The results are displayed in Fig.4.

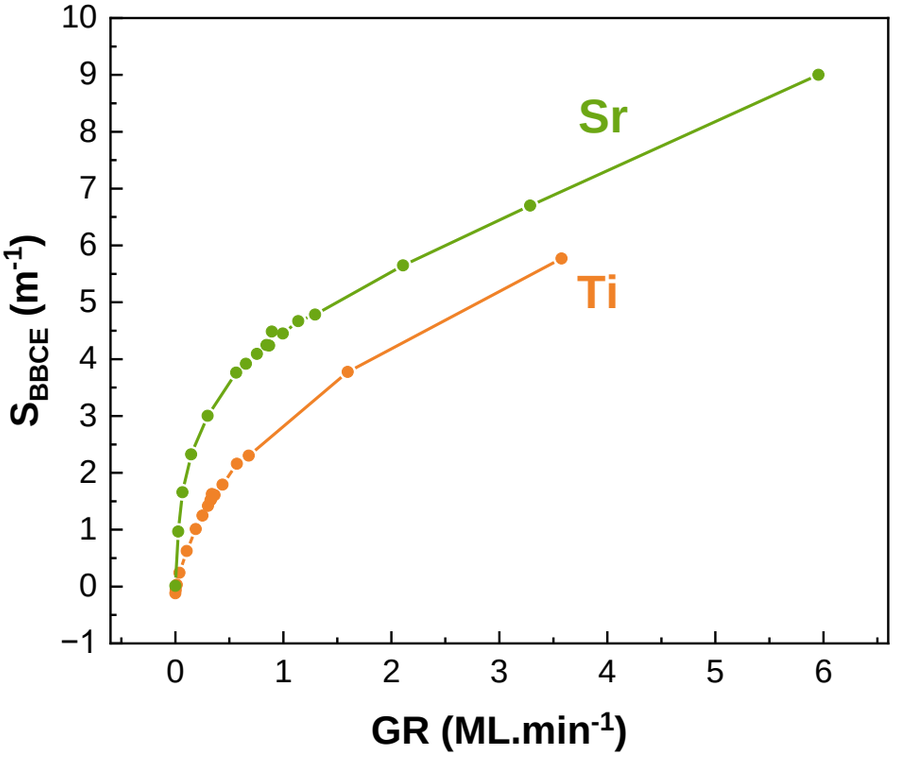

***Fig.4** : S_{BBCE} as a function of GR for Sr and Ti.*

The dependency of S_{BBCE} to GR is not straightforward and will be the object of a dedicated work, where we will in particular show that the sublinear increase of S_{BBCE} with increasing GR is related to the fact that the absorption dips are not spectrally resolved by the monochromator. Yet, S_{BBCE} is larger for Sr than for Ti, due to the larger linestrength of the Sr line[27].Fig.5 compares quantitatively the SNR of our sensor to that of standard OFM sensors.

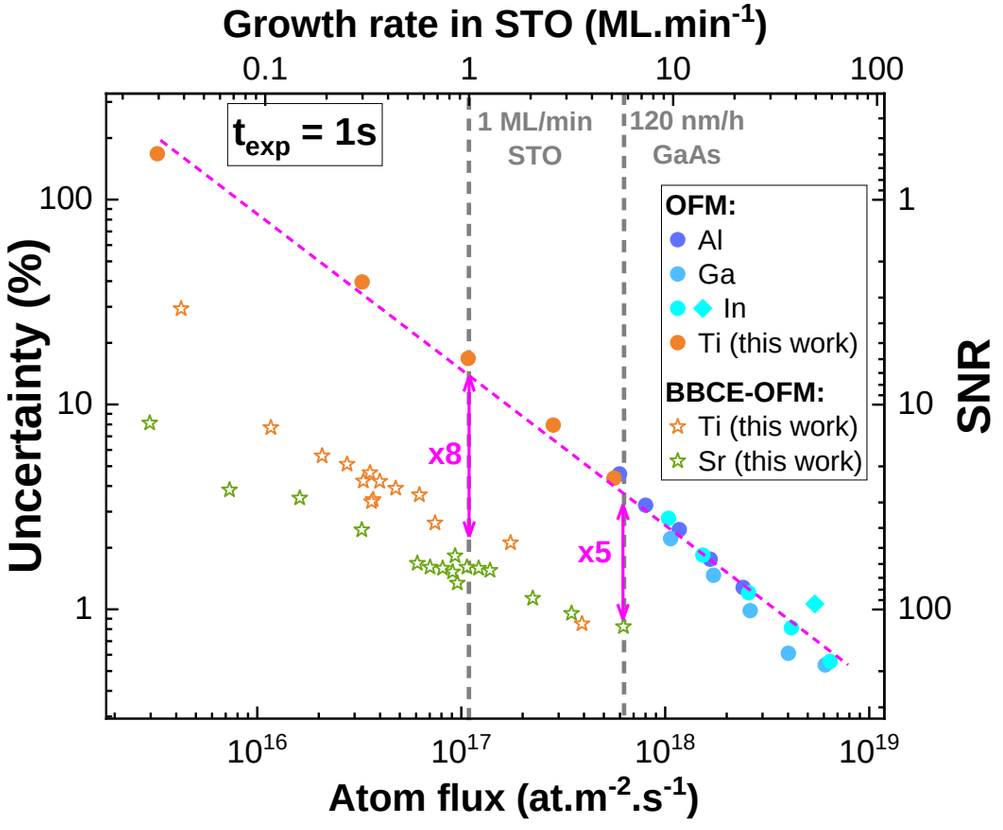

Fig.5*: Comparison of the measurement uncertainties (1σ standard deviation/mean value) obtained with the BBCE-OFM sensor (stars) to that obtained with standard OFM sensors (dots) as a function of the growth rate, for an exposure time of 1s. The data for Al, Ga and In were obtained directly from the graphs in Refs* [17,28].

In this figure, the measurement uncertainty is defined as the ratio between the standard deviation of the signal and its mean value. For standard OFM sensors, the values extracted from our measurement for Ti (orange dots, more details in SM section SM1) are consistent with those available in literature (blue dots). The uncertainty is very large at low growth rate (in the order of ±16% for an STO growth rate of 1 ML/min, for example) and decreases as the growth rate increases. Our BBCE-OFM sensor offers a significant gain in measurement uncertainty compared to standard OFM sensors. This gain is larger at low growth rates. So, for example, standard OFM sensors lead to very high uncertainties in the low growth rate conditions used to fabricate STO (and other perovskite oxides) by MBE, making them barely usable for this application. In contrast, our sensor enables the growth rate of these materials to be monitored with a reasonable accuracy in the % range.

Conclusion

In summary, the implementation of an optical cavity, and the replacement of HCLs by LEDs, enabled by the use of an echelle monochromator without cross-disperser, confer on our BBCE-OFM sensor beyond state-of-the-art performances. The measurement uncertainty is strongly reduced as compared to standard OFM sensors, enabling accurate deposition process monitoring even at very low growth rates. Our next studies will aim to further reduce the measurement uncertainty through a systematic study of the sources of noise. The long-term stability of our sensor has to be assessed, which will also be the subject of future works. The architecture of our sensor, including a single optical path for the absorbed beam and the reference, combined to the high LED stability, offers hope for improved stability compared to standard OFM sensors. In the longer term, our sensor, which can not only monitor atoms but also molecules and excited species in plasma thanks to the LEDs broadband spectra, could be also adapted monitor non-MBE growth processes, such as sputtering, CVD, etc….

Supplementary material

The supplementary material describes the standard OFM setup we used to benchmark BBCE-OFM performances, some details about the echelle spectrometer, a comparison of the spectral radiances of LEDs with that of HCLs, the calculation of the BBCE-OFM sensor response, measurements illustrating the influence of the cell temperature on the absorption line spectral shape and details about the measurement of the sensor signal as a function of the growth rate

Funding. Agence Nationale de la Recherche (CEAS-OFM project [ANR-21-CE24-0003])

Acknowledgments. The authors thank the Nanolyon platform for their support in the MBE experimental work.

Disclosures. The authors declare no conflicts of interest.

Data availability. The data that support the findings of this study are available from the corresponding author upon reasonable request.

References

[1] K. Seshan, *Handbook of Thin Film Deposition* (William Andrew, 2012).

[2] Y.S. Kim, N. Bansal, C. Chaparro, H. Gross, and S. Oh, "Sr flux stability against oxidation in oxide-molecular-beam-epitaxy environment: Flux, geometry, and pressure dependence," Journal of Vacuum Science & Technology A: Vacuum, Surfaces, and Films **28**(2), 271–276 (2010).

[3] L.L. Chang, L. Esaki, W.E. Howard, and R. Ludeke, "The Growth of a GaAs–GaAlAs Superlattice," Journal of Vacuum Science and Technology **10**(1), 11–16 (1973).

[4] C. Lu, and Y. Guan, "Improved method of nonintrusive deposition rate monitoring by atomic absorption spectroscopy for physical vapor deposition processes," Journal of Vacuum Science & Technology A: Vacuum, Surfaces, and Films **13**(3), 1797–1801 (1995).

[5] C. Lu, M.J. Lightner, and C.A. Gogol, "Rate controlling and composition analysis of alloy deposition processes by electron impact emission spectroscopy (EIES)," Journal of Vacuum Science and Technology **14**(1), 103–107 (1977).

[6] T.Y. Kometani, and W. Wiegmann, "Measurement of Ga and Al in a molecular-beam epitaxy chamber by atomic absorption spectrometry (AAS)," Journal of Vacuum Science and Technology **12**(4), 933–936 (1975).

[7] H.C. Wagenaar, I. Novotny, and L. De Galan, "The influence of hollow-cathode lamp line profIles upon analytical curves in atomic absorption spectroscopy," Spectrochimica Acta **29**, 301–317 (1974).

[8] H.C. Wagenaar, and L. De Galan, "Interferometric measurements of atomic line profiles emitted by hollow-cathode lamps and by an acetylene-nitrous oxide flame," Spectrochim Acta Part B At Spectrosc **28**(5), 157–177 (1973).

[9] H. Scheibner, S. Franke, S. Solyman, J.F. Behnke, C. Wilke, and A. Dinklage, "Laser absorption spectroscopy with a blue diode laser in an aluminum hollow cathode discharge," Review of Scientific Instruments **73**(2 I), 378 (2002).

[10] O.M. Maragò, B. Fazio, P.G. Gucciardi, and E. Arimondo, "Atomic gallium laser spectroscopy with violet/blue diode lasers," Applied Physics B **77**(8), 809–815 (2003).

[11] M. Resano, M.R. Flórez, and E. García-Ruiz, "High-resolution continuum source atomic absorption spectrometry for the simultaneous or sequential monitoring of multiple lines. A critical review of current possibilities," Spectrochim Acta Part B At Spectrosc **88**, 85–97 (2013).

[12] A.W. Jackson, P.R. Pinsukanjana, A.C. Gossard, and L.A. Coldren, *Noise, Drift, and Calibration in Optical Flux Monitoring for MBE* (1999).

[13] S.A. Chalmers, and K.P. Killeen, "Real-time control of molecular beam epitaxy by optical-based flux monitoring," Appl Phys Lett **63**(23), 3131–3133 (1993).

[14] S.J. Benerofe, C.H. Ahn, M.M. Wang, K.E. Kihlstrom, K.B. Do, S.B. Arnason, M.M. Fejer, T.H. Geballe, M.R. Beasley, and R.H. Hammond, "Dual beam atomic absorption spectroscopy for controlling thin film deposition rates," Journal of Vacuum Science & Technology B: Microelectronics and Nanometer Structures Processing, Measurement, and Phenomena **12**(2), 1217–1220 (1994).

[15] M.E. Klausmeier-Brown, J.N. Eckstein, I. Bozovic, and G.F. Virshup, "Accurate measurement of atomic beam flux by pseudo-double-beam atomic absorption spectroscopy for growth of thin-film oxide superconductors," Appl Phys Lett **60**(5), 657–659 (1992).

[16] Y. Du, T.C. Droubay, A. V. Liyu, G. Li, and S.A. Chambers, "Self-corrected sensors based on atomic absorption spectroscopy for atom flux measurements in molecular beam epitaxy," Appl Phys Lett **104**(16), (2014).

[17] P. Pinsukanjana, A. Jackson, J. Tofte, K. Maranowski, S. Campbell, J. English, S. Chalmers, L. Coldren, and A. Gossard, "Real-time simultaneous optical-based flux monitoring of Al, Ga, and In using atomic absorption for molecular beam epitaxy," Journal of Vacuum Science & Technology B: Microelectronics and Nanometer Structures Processing, Measurement, and Phenomena **14**(3), 2147–2150 (1996).

[18] D. Romanini, I. Ventrillard, G. Méjean, J. Morville, and E. Kerstel, *Introduction to Cavity Enhanced Absorption Spectroscopy* (Heidelberg: Springer Berlin Heidelberg, 2014).

[19] W.G. Fastie, "Ebert spectrometer reflections," Phys Today **44**(1), 37–43 (1991).

[20] Giel. Berden, and Richard. Engeln, *Cavity Ring-down Spectroscopy : Techniques and Applications* (Wiley, 2009).

[21] D. Vignaud, " Real-time in situ flux monitoring in molecular beam epitaxy by wavelength-modulated atomic absorption spectroscopy ," Journal of Vacuum Science & Technology B: Microelectronics and Nanometer Structures Processing, Measurement, and Phenomena **25**(4), 1398–1404 (2007).

[22] W. Wang, R.H. Hammond, M.M. Fejer, S. Arnason, M.R. Beasley, M.L. Bortz, and T. Day, "Direct atomic flux measurement of electron-beam evaporated yttrium with a diode-laser-based atomic absorption monitor at 668 nm," Appl Phys Lett **71**(1), 31–33 (1997).

[23] C. Palmer, and E.G. Loewen, *Diffraction Grating Handbook* (2005).

[24] Y. Kasai, and S. Sakai, "Atomic absorption spectroscopy system for flux monitoring and atomic-layer control of molecular beam epitaxial growth of BiSrCaCuO," Review of Scientific Instruments **68**(7), 2850–2855 (1997).

[25] R. Rousseau, J. Morville, C. Botella, and G. Saint-Girons, "Absorption line broadening in atomic beams produced in a molecular beam epitaxy environment," Submitted to Optics Express, (n.d.).

[26] S.E. Fiedler, A. Hese, and U. Heitmann, "Influence of the cavity parameters on the output intensity in incoherent broadband cavity-enhanced absorption spectroscopy," Review of Scientific Instruments **78**(7), (2007).

[27] Y. Ralchenko, *NIST Atomic Spectra Database* (2005).

[28] P.R. Pinsukanjana, J.M. Marquis, J. Hubbard, M.A. Trivedi, R.F. Dickey, J.M.S. Tsai, S.P. Kuo, P.S. Kao, and Y.C. Kao, "InGaAs composition monitoring for production MBE by in situ optical-based flux monitor (OFM)," in *J Cryst Growth*, (2003), pp. 124–129.